Proc. Natl. Acad. Sci. USA
Vol. 95, pp. 6624–6629, June 1998
Biochemistry

The design, computer modeling, solution structure, and biological evaluation of synthetic analogs of bryostatin 1

PAUL A. WENDER*†, JEF DEBRABANDER†, PATRICK G. HARRAN†, JUAN-MIGUEL JIMENEZ†, MICHAEL F. T. KOEHLER†, BLAISE LIPPA†, CHEOL-MIN PARK†, CARSTEN SIEDENBIEDEL†, AND GEORGE R. PETTIT‡

†Department of Chemistry, Stanford University, Stanford, CA 94305-5080; and ‡Cancer Research Institute and Department of Chemistry, Arizona State University, Tempe, AZ 85287

Communicated by John I. Brauman, Stanford University, Stanford, CA, March 30, 1998

ABSTRACT **The bryostatins are a unique family of emerging cancer chemotherapeutic candidates isolated from marine bryozoa. Although the biochemical basis for their therapeutic activity is not known, these macrolactones exhibit high affinities for protein kinase C (PKC) isozymes, compete for the phorbol ester binding site on PKC, and stimulate kinase activity *in vitro* and *in vivo*. Unlike the phorbol esters, they are not first-stage tumor promoters. The design, computer modeling, NMR solution structure, PKC binding, and functional assays of a unique class of synthetic bryostatin analogs are described. These analogs (7b, 7c, and 8) retain the putative recognition domain of the bryostatins but are simplified through deletions and modifications in the C4-C14 spacer domain. Computer modeling of an analog prototype (7a) indicates that it exists preferentially in two distinct conformational classes, one in close agreement with the crystal structure of bryostatin 1. The solution structure of synthetic analog 7c was determined by NMR spectroscopy and found to be very similar to the previously reported structures of bryostatins 1 and 10. Analogs 7b, 7c, and 8 bound strongly to PKC isozymes with K_i = 297, 3.4, and 8.3 nM, respectively. Control 7d, like the corresponding bryostatin derivative, exhibited weak PKC affinity, as did the derivative, 9, lacking the spacer domain. Like bryostatin, acetal 7c exhibited significant levels of *in vitro* growth inhibitory activity (1.8–170 ng/ml) against several human cancer cell lines, providing an important step toward the development of simplified, synthetically accessible analogs of the bryostatins.**

The bryostatins (Fig. 1) comprise a structurally and functionally novel group of 20 macrocyclic lactones originally isolated from *Bugula neritina* and other marine bryozoa on the basis of their significant activity against murine P388 lymphocytic leukemia (1). These macrocycles subsequently have been identified as important leads in cancer chemotherapy, and bryostatin 1 recently has entered phase II human clinical trials for the treatment of melanoma, non-Hodgkins lymphoma, and renal cancer (current information on bryostatin clinical trials can be found on the Web at: http://cancernet.nci.nih.gov/prot/protsrch.shtml). This compound continues to be evaluated in phase I clinical trials, alone and in combination with other drugs, for the treatment of other types of cancer (2). Adding to the interest in the bryostatins is their unique biochemistry. Bryostatin 1 has been found to promote the normal growth of bone marrow progenitor cells (3, 4), to provide *in vivo* protection against normally lethal doses of ionizing radiation (5), and to serve as an immune stimulant, effecting the normal production of interleukin 2 and interferon.

Unfortunately, the low natural abundance of the bryostatins and difficulties associated with their isolation have impeded efforts to elucidate their molecular mode of action and to accelerate their clinical development. The initial isolation of bryostatin 1 from *B. neritina*, for example, required 500 kg of wet animals (1, 2) to obtain sufficient material for structural characterization and bioassay. Subsequent isolations of this and other bryostatins have produced yields ranging from 10^{-3} to 10^{-8}% (2). In an effort to generate adequate material for human therapeutic use, large-scale aquaculture of *B. neritina* currently is being investigated (6). However, at present, the supply of these molecules for research and clinical studies continues to be limited.

The biochemical basis for the therapeutic effects of bryostatin is not established. However, the bryostatins are known to competitively inhibit the binding of phorbol esters to protein kinase C (PKC) at low nanomolar to picomolar concentrations (7) and to stimulate comparable kinase activity *in vitro* (8–10). Notably, however, they induce only a subset of typical phorbol ester responses and block those actions of phorbol esters that they themselves do not initiate. Examples include differentiation in HL-60 promyelocytic leukemia cells (8, 11) and in Friend erythroleukemia cells (12), proliferation of JB6 mouse epidermal cells (13), arachidonic acid release in C3H10T1/2 cells (14), and first-stage tumor promotion in mouse skin (15). An understanding of the structural basis for these and other bryostatin activities is central to the development of simpler, clinically superior chemotherapeutic agents and to the advancement of their use as probes in the PKC signal transduction cascade.

In 1988, the groups of Wender, Blumberg, and Pettit (16) reported that a proposed pharmacophoric model for PKC agonists could be used to rationalize how the structurally dissimilar bryostatins, phorbol esters, and 1,2-diacyl-*sn*-glycerol (DAG), the endogenous PKC activator (17), might compete for the same site on PKC. Although the existence of a common pharmacophore is not required for competitive binding, this hypothesis served as a testable starting point for rationalizing the binding behavior of these natural products. Toward this end, the interatomic distances of all possible heteroatomic triads in the relatively rigid phorbol esters were compared with heteroatomic triad distances in low-energy conformers of DAG. The best correlation from this analysis mapped onto the C1 carbonyl, the C19 hydroxyl group, and the C26 hydroxyl group of bryostatin 1 (Fig. 2). Other correlations were identified and ranked from comparable to weak.

The resulting hypothesis, and the starting point for the current study, was that the A and B rings of bryostatin could

The publication costs of this article were defrayed in part by page charge payment. This article must therefore be hereby marked "*advertisement*" in accordance with 18 U.S.C. §1734 solely to indicate this fact.

Abbreviations: PKC, protein kinase C; DAG, 1,2- diacyl-*sn*-glycerol.

*To whom reprint requests should be addressed. e-mail: wender@saurus.stanford.edu.

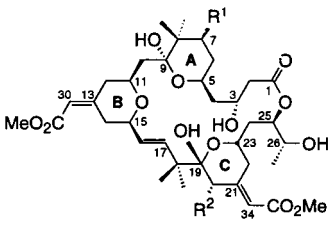

Entry	Bryostatin	R^1	R^2	K_i (x 10^{-9} M†)
1	1	O_2CCH_3		1.35 ± 0.17
2	2	OH		5.86 ± 1.13
3	3*			2.75 ± 0.05
4	4	$O_2CC(CH_3)_3$	$O_2CCH_2CH_2CH_3$	1.30 ± 0.19
5	5	$O_2CC(CH_3)_3$	O_2CCH_3	1.04 ± 0.10
6	6	$O_2CCH_2CH_2CH_3$	O_2CCH_3	1.18 ± 0.29
7	7	O_2CCH_3	O_2CCH_3	0.84 ± 0.07
8	8	$O_2CCH_2CH_2CH_3$	$O_2CCH_2CH_2CH_3$	1.72 ± 0.10
9	9	O_2CCH_3	$O_2CCH_2CH_2CH_3$	1.31 ± 0.00
10	10	$O_2CC(CH_3)_3$	H	1.56 ± 0.16‡
11	2 (13,30,2',3',4',5'-hexahydro)			9.61 ± 0.94
12	2 (13,30,21,34,2',3',4',5'-octahydro)			473 ± 96
13	4 (13,30-epoxide)			0.54 ± 0.07
14	1 (26-epi)			32.6 ± 6.6‡
15	4 (26-acetate)			>>100

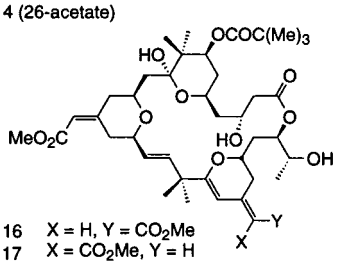

16	16	X = H, Y = CO_2Me	118 ± 2‡
17	17	X = CO_2Me, Y = H	188 ± 7‡

* Revised structure from ref. 27
† Mean ± range (n=2) or ± SEM (n>2). Ref. 18
‡ Competitive binding to recombinant PKC α. See Ref. 30

FIG. 1. Structure and PKC binding affinities of the bryostatins and selected semisynthetic derivatives.

serve partly as spacers to remotely control the orientation and mobility of the groups (C1, C19, and C26) putatively required for recognition. This hypothesis was consistent with the then-known bryostatin structure-activity relationships and continues to be in agreement with recent studies on newly discovered bryostatins (18, 19). Notably, it also has found utility in the *de novo* design of new PKC activators (20). This hypothesis now has been used in the design of simplified, fully synthetic bryostatin analogs that retain PKC binding affinity and, in the case examined, possess significant levels of *in vitro* cell growth inhibitory activity.

MATERIALS AND METHODS

Synthetic Bryostatin Analogs and Controls. Compounds **7b-d**, **8** and **9** (see Fig. 5) were prepared and purified according to the general strategy outlined in Fig. 3*A*. All compounds gave analytical data in full agreement with their reported structures. Experimental details will be described in a separate disclosure (21).

PKC Binding Assays. PKC was obtained from DEAE-cellulose chromatography of rat brain cytosol and 1% Triton-extracted particulate fractions as described previously (22). Competitive binding of synthetic analogs to the mixture of PKC isozymes was carried out according to Tanaka *et al.* (23). Briefly, a standard buffer solution was freshly prepared for each assay, which contained 50 mM Tris·HCl, 100 mM KCl, and 2 mg/ml BSA. A portion of this mixture was set aside and

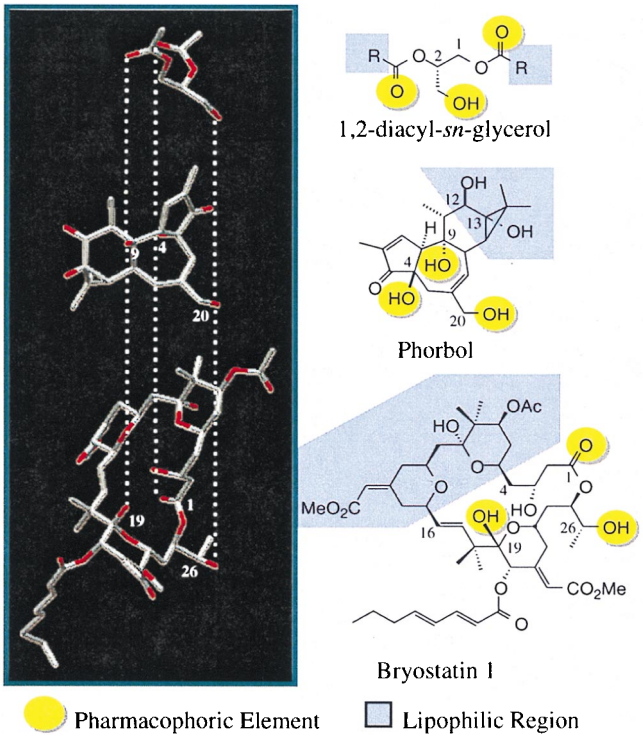

FIG. 2. Calculated low-energy conformers of DAG (*Top*), x-ray structures of phorbol (*Middle*), and bryostatin 1 (*Bottom*). The vertical dashed lines connect heteroatoms (potential recognition elements) whose relative spatial coordinates are comparable in each structure. The lipophilic region is truncated in DAG and omitted in phorbol for clarity. This region is occupied by the esters (R) in DAG, C12, C13-diesters in phorbol, and the C4-C16 segment of bryostatin 1.

1 mg/ml of phosphatidyl serine (PS; 1,2-di-(cis-9-octadecenoyl)-*sn*-glycero-3-phospho-L-serine, Avanti Polar Lipids) was added to it, and the resultant mixture was sonicated four times for 30 sec at 0°C, pausing 30 sec between cycles. To the remaining buffer was added ≈0.1 unit/ml of PKC. Reaction vials were prepared by successively adding 60 μl of the PS-containing buffer, 200 μl of the PKC-containing buffer, 20 μl of the compound to be assayed, and 20 μl of 150 nM C20-tritiated phorbol-12,13-dibutyrate ([^{3}H]PDBu) (DuPont/NEN) in a 2.5% dimethyl sulfoxide/H_2O solution. Unlabeled phorbol 12-myristate 13-acetate was added to a concentration of 17 μM to tubes used to measure nonspecific binding. The vials were incubated at 37°C for 100 min and then placed on ice for 5 min. The samples were filtered and washed as previously described (23). The filters were soaked for 12 hr in 3 ml of CytoScint scintillation fluid before counting. Counts per minute were averaged among three trials at each concentration.

NMR Spectroscopy and Molecular Modeling. Proton NMR spectra were recorded at 500 MHz in C_6D_6 or $CDCl_3$ solution on a Varian Unity 500 operating at 25°C. After conversion from their native format, free inductive decays (FIDs) were processed and analyzed with FELIX 95.0 (Biosym Technologies, San Diego) on a Silicon Graphics R5000 Indy workstation. Each FID was zero-filled to 1,024 points and apodized with a 90° phase-shifted sinebell squared function before Fourier transformation. The first points of the FIDs were multiplied by 0.5 before transformation in t1.

Proton assignments were made by using double quantum-filtered correlated spectroscopy (DQF-COSY), total correlation spectroscopy (TOCSY), and nuclear Overhauser effect spectroscopy (NOESY) spectra. NOESY cross-peak volumes in the 100-ms mixing time spectrum were measured within FELIX, normalized to the weakest crosspeak, and then divided into strong, medium, and weak categories. The methyl cross-

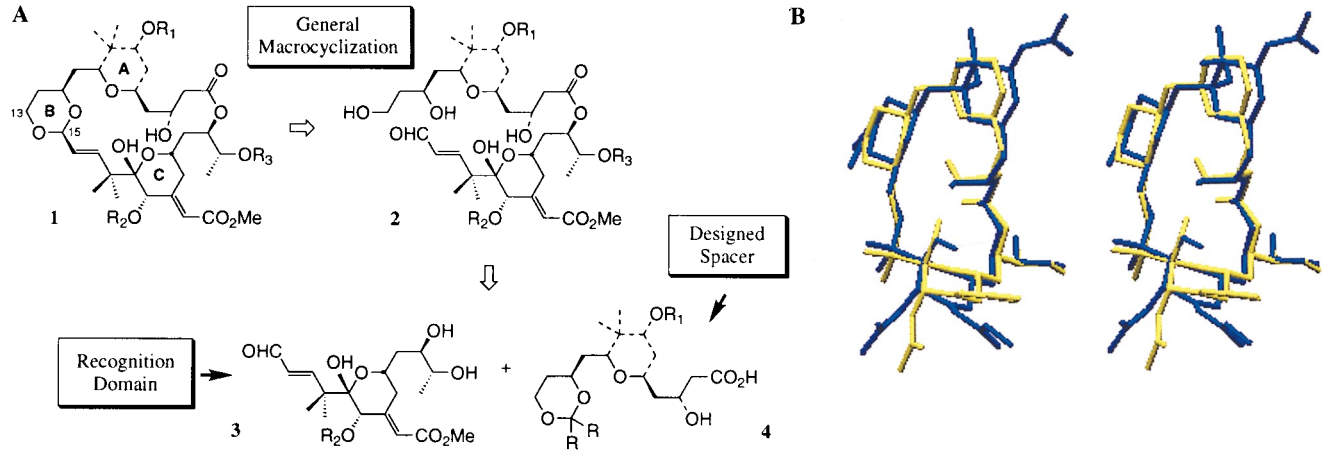

FIG. 3. (*A*) A convergent synthetic strategy for the preparation of macrocyclic acetal analogs of the bryostatins. Dashed lines correspond to bonds that might not be required in the spacer domain. (*B*) Stereoview of the superimposition of the crystal structure of bryostatin 1 (blue) and a conformer of **7a** (yellow) calculated to be 2.17 kcal/mol above the global minimum. rms deviation = 0.131 Å between the C1, C19, and C26 oxygen atoms of the superimposed structures. The C20 side chain in bryostatin 1 is depicted as the acetate for clarity.

peak volumes were divided by three before normalization (24). The cross-peak intensities then were converted to internuclear distance constraints and applied to the lowest energy structure produced from molecular modeling of compound **7a.** Strong constraints were allowed to vary between 1.8 and 2.5 Å without an energy penalty, medium between 1.8 and 3.5 Å, and weak between 1.8 and 5.0 Å. The constrained structure then was subjected to a constrained molecular dynamics simulation at 900°K, using MACROMODEL V.4.5 (25). Chloroform solvation was simulated in all calculations by the generalized Born/solvent accessible surface area model (26). The structure was brought to 900°K over 10 ps, then equilibrated for 10 ps with a time step of 1.0 fs. One thousand structures were sampled during a subsequent 100-ps simulation, also at 900°K with a 1.0-fs time step. These structures then were minimized to convergence by using a maximum of 2,000 iterations of truncated Newton conjugate gradient minimization. The NMR constraints remained in place throughout this minimization.

RESULTS AND DISCUSSION

Analog Design. Because of the limited availability of the natural bryostatins and the difficulties encountered in their selective modification, structure-activity studies thus far have been largely confined to the natural products themselves and closely related derivatives. These studies, however, have revealed some information pertinent to the design of analogs. Comparisons of the PKC binding affinities of bryostatins 1–10 indicate that changes in the R^1 and R^2 groups have only a modest effect on binding (Fig. 1, entries 1–10). Similarly, analogs derived from reduction or epoxidation of the C13-C30 alkene still retain significant affinity (Fig. 1, entries 11 and 13). In contrast, analogs in which both the C13-C30 and C21-C34 alkenes are hydrogenated showed markedly reduced affinities (Fig. 1, entry 12). Elimination of the C19 hydroxyl group (Fig. 1, entries 16 and 17) or inversion of stereochemistry at C26 (Fig. 1, entry 14) have a more pronounced effect on affinity. Finally, acetylation at C26 eliminates significant binding (Fig. 1, entry 15). Viewed collectively, these observations suggest that the binding of the bryostatins is only modestly affected by changes in the C4-C16 domain but diminished significantly by alterations in the C19-C26 domain.

The structure-activity relationships and computer modeling of the bryostatins (Fig. 2) suggest that bryostatin-like recognition could be achieved in analogs that retain the recognition domain functionality but incorporate simplified spacers (C4-C16). The structure of the spacer could, in principle, be varied as needed to simplify synthesis and to tune pharmacokinetic performance provided that its functional role in orienting and constraining the recognition domain is maintained (19). A first-generation analog family (Fig. 3*A*) was designed to explore this hypothesis. To compare systematically the role of the spacer domain in these designed analogs with that of the bryostatins, the recognition domain of the bryostatins was kept intact in the designed analogs. Functionality along the C7-C13 periphery of the molecule was completely eliminated, and C14 was replaced by an oxygen to facilitate synthesis. The resulting target macrocyclic acetals (Fig. 3*A*, **1**) were seen as the products of an acid-catalyzed intramolecular acetalization of intermediate *seco*-aldehydes **2**, themselves constructed from the esterification of carboxylic acids of general structure **4** with bryostatin fragment **3**. From a synthetic standpoint this approach was attractive in several significant ways: first, macroacetalization represents a unique (28) and potentially general solution for closing the 23-membered lactone with control of relative stereochemistry at C15; second, the strategy is highly convergent and devoid of demanding carbon–carbon bond constructions late in the synthesis, and third, the proposed chemistry is expected to tolerate a wide variety of acetals **4** without complication. Finally, this strategy potentially could be used to create analog libraries through combinatorial synthesis involving the coupling of fragment **3** with various readily available acid-acetals.

To rapidly evaluate the conformational correspondence between the designed analogs and bryostatin, the conformations of the analogs first were determined by molecular mechanics calculations and compared with the known solid-state and solution structures of the bryostatins. Prototypical compound **7a** was subjected to an extensive search of its conformational space within the multiconformer mode of the MM2 force field provided with MACROMODEL V.4.5 (25). Ten thousand conformers of this analog were randomly generated and minimized by using the truncated Newton conjugate gradient.

Water solvation was simulated by the generalized Born/solvent accessible surface area model (26). A total of 2,784 unique conformations were found and minimized to good convergence, a process whose effectiveness was evident from the fact that only two new conformers within 2 kcal/mol of the global minimum were found in the final 2,500 iterations. The lowest energy structures from this analysis fell into two distinct conformational families, which subsequently were examined for similarity to the known solid-state structure of bryostatin 1 and the closely related solution structure of bryostatin 10 (29). Interestingly, relative to bryostatin 1, each member of the family containing the calculated global minimum was substantially distorted because of a characteristic hydrogen bond

between the C3 hydroxyl group and the adjacent C1 lactone carbonyl. However, the second low-energy conformational family, whose members began appearing at energies 1.9 kcal/mol above the global minimum, displayed an internal hydrogen bonding pattern consistent with that observed in natural bryostatins; namely, the C19 hemiketal participating in a transannular hydrogen bond to the C3 alcohol, which is, in turn, similarly bonded to the oxygen atom of the B-ring pyran. Fig. 3*B* depicts the crystal structure of bryostatin 1 superimposed onto a representative member of this second conformational family calculated for **7a**, which is 2.17 kcal/mol higher in energy than the global minimum. Comparison of the putative pharmacophoric elements (C1, C19, and C26 heteroatoms) between the two structures gives a rms deviation of 0.131 Å. Interestingly, submitting bryostatin 1 (C20 acetate) to an identical computation produced two families of low-energy conformations directly analogous to those found for **7a**. Thus, both visually and by calculation, a low-energy computed structure of the designed analog was found to exhibit a good correspondence with the experimentally established structures of bryostatins.

Bryostatin analogs **7b** and **7c** were synthesized according to the general strategy outlined in Fig. 3*A* (21). Acetate **7d** was synthesized to function as a negative control, analogous to the corresponding bryostatin derivative, which does not bind PKC significantly. Analog **8**, in which the spacer domain is further simplified through replacement of the A-ring pyran with a conformationally restricting *tertiary*-butyl group, was constructed by using a similar synthetic strategy. Finally, compound **9**, which incorporates the recognition domain but not the spacer domain, was prepared as an additional control to test the role of the spacer in orienting the recognition elements (see Fig. 5).

Solution Structure of Acetal 7c. Comparison of the computed structures of the designed compounds with known solution and solid-state structures of bryostatins served as a rapid, preliminary screen for the identification of potential analog candidates. The synthesis of the qualifying candidates subsequently allowed for a direct determination of their solution structure. For this purpose, acetal **7c** was subjected to a series of high field one- and two-dimensional proton NMR experiments. The reported solution structure of bryostatin 10 (29) served as a reference point. A close correlation between ^{1}H chemical shifts and multiplicities in $CDCl_3$ between **7c** and bryostatin 10 was observed throughout most of the putative pharmacophoric region (C16 through C23). The lack of signal resolution between 1 and 2 ppm (downfield from tetramethylsilane) caused by the greater number of aliphatic protons in structure **7c** relative to bryostatin 10 was resolved by changing the solvent to C_6D_6. In this case, all crucial resonances and their splitting patterns were uniquely assigned.

These resonances appeared as a single set of sharp spectral lines with coupling constants that deviated significantly from rotationally averaged values, indicating that compound **7c** existed predominantly as a single, stable conformer at room temperature. Phase-sensitive nuclear Overhauser effect spectroscopy (NOESY), total correlation spectroscopy (TOCSY), and double quantum-filtered correlated spectroscopy (DQF-COSY) spectra of compound **7c** in C_6D_6 were analyzed to determine the identity and categorical distances between protons throughout the structure. From this analysis, 33 unique internal distance constraints were generated and subsequently applied to the lowest energy conformation originally calculated for acetal **7a**. Before molecular dynamics simulation, this calculated structure was inconsistent with the NMR data as five imposed distance constraints were violated by >0.25 Å (dashed lines in Fig. 4*A*). Subsequent constrained gas-phase molecular dynamics simulation followed by minimization identified 95 unique conformers, six of which were within 2 kcal/mol of the global minimum. The low energy

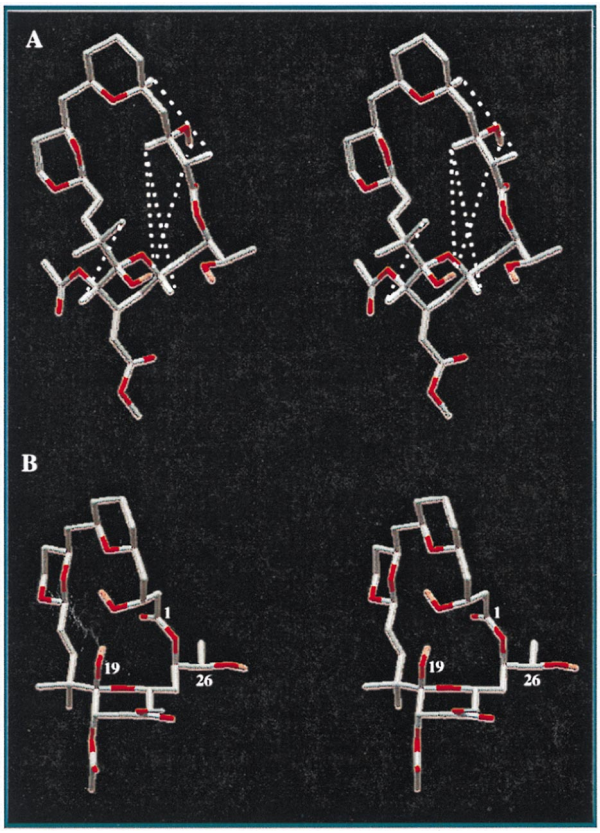

FIG. 4. (*A*) Stereoview of lowest-energy conformer originally calculated for **7a**. Dashed lines connect protons whose internuclear distances are inconsistent with nuclear Overhauser effect data observed for **7c** (violation ≥ 0.5 Å). (*B*) Stereoview of a conformation of **7a** 2.1 kcal/mol above the global minimum) fully concordant with the NMR data.

conformers satisfied all the nuclear Overhauser effect constraints applied to them and compared favorably with the published crystal structure of bryostatin 1 as well as the solution structure of bryostatin 10. As was observed in the crystal structure, two rotomers about the C25-C26 bond were observed, one being the lowest-energy conformer, and the other appearing 2.1 kcal/mol higher in energy. Superimposition of the lowest-energy conformer and the crystal structure of bryostatin 1 (all heavy atom comparison) gave a rms deviation of 0.506 Å. The rms deviation calculated by superimposing the pharmacophoric atoms of our lowest-energy conformer onto their counterparts in bryostatin 1 is 0.313 Å, indicating a remarkably good correlation between the two in their ability to present the putative pharmacophoric triad to PKC.

PKC Binding Assays of Synthetic Bryostatin Analogs and Controls. Analogs **7b**, **7c**, and **8** and controls **7d**, and **9** were evaluated for their ability to bind to a mixture of rat brain PKC isozymes. A competition assay with C20-tritiated phorbol-12,13-dibutyrate was selected to determine the relative binding affinities of these compounds because of the wealth of information on this PKC binding standard, its previous use in determining the binding of bryostatins, and its ready availability. Analogs **7b**, **7c**, and **8** were found to bind in a specific, saturable manner with the inhibition constants (K_i) shown in Fig. 5. Controls **7d** and **9** exhibited at best weak affinity for PKC over the range studied. In each case, K_i was calculated from the 50% inhibitory concentration (IC_{50}) obtained from a nonlinear regression plot of average cpm versus [analog]. Nonspecific binding was determined at [phorbol 12-myristate

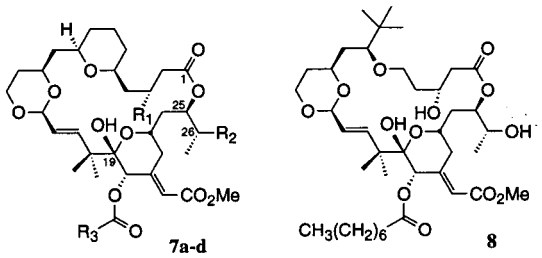

Compound	R_1	R_2	R_3	K_i (x 10^{-9} M)
7a	OH	OH	CH_3	------
7b	H	OH	$(CH_2)_6CH_3$	297 ± 29
7c	OH	OH	$(CH_2)_6CH_3$	3.4 ± 0.6
7d	OH	OAc	$(CH_2)_6CH_3$	>10000
8				8.3 ± 0.2
9				>10000

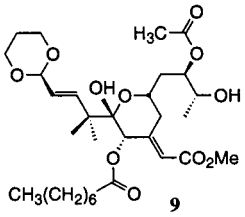

FIG. 5. The structures and PKC binding affinities of synthetic bryostatin analogs and controls.

13-acetate] = 17 μM and the K_d of [^{3}H]PDBu was determined, under identical assay conditions, to be 1.3 nM (23).

Growth Inhibitory Activities of Analog 7c. For details of the known cancer cell line evaluations shown in Table 1 refer to ref. 31.

DISCUSSION

The bryostatins elicit a range of unique biochemical responses and are promising candidates for the treatment of cancer. However, relatively little is known about their molecular mode of action. Structure-activity studies have been limited by the lack of material and the difficulties arising in the selective modification of the complex bryostatin functionality. The current study was designed to provide insights on the structural features of the bryostatins that contribute to their activity, in this case, binding to PKC. This approach in turn serves to establish the information needed to design simpler and potentially superior clinical candidates that could be made through practical synthesis.

Because the role of these marine-derived macrocycles in mammalian biochemistry is determined in part by the spatial array of their recognition elements, a computer search initially was conducted to identify possible common recognition elements in the bryostatins and other compounds that compete with the bryostatins for binding to PKC. Several arrays of common functionality were identified and prioritized based on distance correlations, with the best correlation corresponding to the oxygens at C1, C19, and C26 in bryostatin 1, a finding in agreement with current structure-activity relationships. This analysis suggested further that bryostatin binding is a cooperative event between two functional domains: one, the recognition domain, containing elements that contact the receptor, and a second, a spacer, which serves to properly orient and constrain the recognition domain.

Table 1. *In vitro* cell growth inhibitory activity of analog **7c**

Human cancer cell line	GI_{50} μg/ml
BXPC-3 (pancreas)	6.0×10^{-3}
NCI-H460 (lung-nonsmall cell)	1.2×10^{-1}
FADU (pharynx)	1.8×10^{-3}
DU-145 (prostate)	1.7×10^{-1}

Designed analogs **7b**, **7c**, and **8** incorporate the recognition domain and simplified spacer domain surrogates of bryostatin 1. Extensive computational analysis of the conformations available to the prototype **7a**, differing from **7c** only at C20 to facilitate calculations, revealed a preference for two low-energy conformational families, one corresponding reasonably well to the known solid-state structure of bryostatin 1. This computer evaluation provided a quick screen for potentially active analogs, leading in this case to the selection and synthesis of **7b**, **7c**, and **8**. The solution structure of acetal **7c** reveals that the replacement of C14 by oxygen and deletion of substituents at C7, C8, C9, and C13 does not alter the ground state conformational preference of the macrocycle relative to the natural products. To determine whether these changes have an effect on the active or recognized conformation, the designed analogs were evaluated for their ability to bind PKC isozymes in competition with tritiated phorbol esters, an assay previously established for the bryostatins. All three analogs bound, with K_is as low as 3.4 and 8.3 nanomolar. These affinities are consistent with those observed for bryostatins 1–10 (Fig. 1) and are better than the affinities determined for bryostatins 17 and 18. In the one case (analog **7c**) studied thus far, it was possible to conduct a functional assay involving growth inhibition against several human cancer cells lines, and significant activity was observed against the cell lines studied.

Further similarities to the bryostatins were observed on modification of the analogs. Thus, like bryostatin 1, the C26 acetate **7d** exhibited no detectable binding under the assay conditions. The absence of significant binding for analog **9** indicates that the recognition elements alone are necessary but insufficient for recognition. As expected, the spacer is required as well to orient and constrain the recognition features for optimal association. The sharply decreased affinity of **7b** relative to **7c** indicates that the C3 hydroxy group plays a significant role in this orientation. Molecular modeling studies and the solution structure of analog **7c** are consistent with the formation of a transannular hydrogen bonding network involving the C3 and C19 hydroxyl groups as well as one of the B ring acetal oxygens.

Analog **8,** which lacks the A-ring but assumes a similar calculated conformation to the other analogs because of the orienting influence of the tertiary-butyl group, is the simplest of the analogs examined and also exhibits potent binding activity.

The low natural abundance and clinical utility of the bryostatins has made all but the simplest alterations of their structures inaccessible, leaving many questions concerning the molecular basis for their cellular effects unaddressed. The demonstration that simplified analogs can emulate the solution and binding behavior of the bryostatins and, in one case, their functional activity is an important step in the design of truly simple, clinically superior agents based on the bryostatin structure. In addition, these synthetically accessible compounds allow further evaluation of the structural basis for the activity of the bryostatins and their molecular mode of action.

We thank Drs. Jean-Charles Chapuis and Jean M. Schmidt for assistance with the known cancer cell line evaluations and Professor Daria Mochly-Rosen for providing laboratory facilities for our binding assays. Financial support of this work was provided by a grant from the National Institutes of Health to P.A.W. (CA31845). Postdoctoral fellowships to J.D. (Fulbright-Hays/North Atlantic Treaty Organization), P.G.H. (National Institutes of Health), J.-M.J. (Fulbright/Spanish Ministry of Education and Science), C.-M.P. (Korean Science and Engineering Foundation), C.S. (Alexander von Humboldt Foundation), and Eli Lilly graduate fellowships to M.F.T.K. and B.L. are gratefully acknowledged.

1. Pettit, G. R., Herald, C. L., Doubek, D. L., Herald, D. L., Arnold, E. & Clardy, J. (1982) *J. Am. Chem. Soc.* **104,** 6846–6848.
2. Pettit, G. R. (1996) *J. Nat. Prod.* **59,** 812–821.
3. Scheid, C., Prendiville, J., Jayson, G., Crowther, D., Fox, B., Pettit, G. R. & Stern, P. L. (1994) *Cancer Immunol. Immunother.* **39,** 223–230.
4. Berkow, R. L., Schlabach, L., Dodson, R., Benjamin, W. H., Pettit, G. R., Rustagi, P. & Kraft, A. S. (1993) *Cancer Res.* **53,** 2810–2815.
5. Pettit, G. R., Gao, F., Sengupta, D., Coll, J. C., Herald, C. L., Doubek, D. L., Schmidt, J. M., Van Camp, J. R., Rudloe, J. J. & Nieman, R. A. (1991) *Tetrahedron* **47,** 3601–3610.
6. Rouhi, A. M. (1995) *Chem. Eng. News*, **73,** 42–44.
7. De Vries, D. J., Herald, C. L., Pettit, G. R. & Blumberg, P. M. (1988) *Biochem. Pharmacol.* **37,** 4069–4073.
8. Kraft, A. S., Smith, J. B. & Berkow, R. L. (1986) *Proc. Natl. Acad. Sci. USA* **83,** 1334–1338.
9. Berkow, R. L. & Kraft, A. S. (1985) *Biochem. Biophys. Res. Commun.* **131,** 1109–1116.
10. Ramsdell, J., Pettit, G. R. & Tashjian, A., Jr. (1986) *J. Biol. Chem.* **261,** 17073–17080.
11. Stone, R. M., Sariban, E., Pettit, G. R. & Kufe, D. W. (1986) *Blood* **68,** 193a (abstr.).
12. Dell'Aquila, M. L., Nguyen, H. T., Herald, C. L., Pettit, G. R. & Blumberg, P. M. (1987) *Cancer Res.* **47,** 6006–6009.
13. Sako, T., Yuspa, S. H., Herald, C. L., Pettit, G. R. & Blumberg, P. M. (1987) *Cancer Res.* **47,** 5445–5450.
14. Dell'Aquila, M. L., Herald, C. L., Kamano, Y., Pettit, G. R. & Blumberg, P. M. (1988) *Cancer Res.* **48,** 3702–3708.
15. Gschwendt, M., Fürstenberger, G., Rose-John, S., Rogers, M., Kittstein, W., Pettit, G. R., Herald, C. L. & Marks, F. (1988) *Carcinogenesis* **9,** 555–562.
16. Wender, P. A., Cribbs, C. M., Koehler, K. F., Sharkey, N. A., Herald, C. L., Kamano, Y., Pettit, G. R. & Blumberg, P. M. (1988) *Proc. Natl. Acad. Sci. USA* **85,** 7197–7201.
17. Nishizuka, Y. (1984) *Nature (London)* **308,** 693–698.
18. Pettit, G. R., Gao, F., Blumberg, P. M., Herald, C. L., Coll, J. C., Kamano, Y., Lewin, N. E., Schmidt, J. M. & Chapuis, J.-C. (1996) *J. Nat. Prod.* **59,** 286–289.
19. Pettit, G. R., Sengupta, D., Blumberg, P. M., Lewin, N. E., Schmidt, J. M. & Kraft, A. S. (1992) *Anti-Cancer Drug Des.* **7,** 101–113.
20. Wender, P. A., Koehler, K. F., Sharkey, N. A., Dell'Aquila, M. L. & Blumberg, P. M. (1986) *Proc. Natl. Acad. Sci. USA* **83,** 4214–4218.
21. Wender, P. A., DeBrabander, J., Harran, P. G., Jimenez, J. M., Koehler, M. F. T., Lippa, B., Park, C. M. & Shiozaki, M. (1998) *J. Am. Chem. Soc.,* in press.
22. Mochly-Rosen, D. & Koshland, D. E., Jr. (1986) *J. Biol. Chem.* **262,** 2291–2297.
23. Tanaka, Y., Miyake, R., Kikkawa, U. & Nishizuka, Y. (1986) *J. Biochem.* **99,** 257–261.
24. Yip, P. F. (1990) *J. Magn. Reson.* **90,** 382–383.
25. Mohamadi, F., Richards, N. G. J., Guida, W. C., Liskamp, R., Lipton, M., Caufield, C., Chang, G., Hendrickson, T. & Still, W. C. (1990) *J. Comput. Chem.* **11,** 440–467.
26. Still, W. C., Tempczyk, A., Hawley, R. C. & Hendrickson, T. (1990) *J. Am. Chem. Soc.* **112,** 6127–6129.
27. Chmurny, G. N., Koleck, M. P. & Hilton, B. D. (1992) *J. Org. Chem.* **57,** 5260–5264.
28. Li, G. & Still, W. C. (1993) *J. Am. Chem. Soc.* **115,** 3804–3805.
29. Kamano, Y., Zhang, H.-P., Morita, H., Itokawa, H., Shirota, O., Pettit, G. R., Herald, D. L. & Herald, C. L. (1996) *Tetrahedron* **52,** 2369–2376.
30. Szallasi, Z., Du, L., Levine, R., Lewin, N. E., Nguyen, P. N., Williams, M. D., Pettit, G. R. & Blumberg, P. M. (1996) *Cancer Res.* **56,** 2105–2111.
31. Pettit, G. R., Srirangam, J. K. S., Barkoczy, J., Williams, M. D., Durkin, K. P. M., Boyd, M. R., Bai, R., Hamel, E., Schmidt, J. M. & Chapuis, J.-C. (1995) *Anti-Cancer Drug Des.* **10,** 529–544.